

NEOWISE Reactivation Mission Year Two: Asteroid Diameters and Albedos

C. R. Nugent¹, A. Mainzer², J. Bauer², R. M. Cutri¹, E. A. Kramer², T. Grav³, J.
Masiero², S. Sonnett², and E. L. Wright⁴

Received _____; accepted _____

¹Infrared Processing and Analysis Center, California Institute of Technology, Pasadena,
CA 91125, USA

²Jet Propulsion Laboratory, California Institute of Technology, Pasadena, CA 91109 USA

³Planetary Science Institute, Tucson, AZ

⁴Department of Physics and Astronomy, University of California, Los Angeles, CA 90095,
USA

ABSTRACT

The Near-Earth Object Wide-Field Infrared Survey Explorer (NEOWISE) mission continues to detect, track, and characterize minor planets. We present diameters and albedos calculated from observations taken during the second year since the spacecraft was reactivated in late 2013. These include 207 near-Earth asteroids and 8,885 other asteroids. 84% of the near-Earth asteroids did not have previously measured diameters and albedos by the NEOWISE mission. Comparison of sizes and albedos calculated from NEOWISE measurements with those measured by occultations, spacecraft, and radar-derived shapes shows accuracy consistent with previous NEOWISE publications. Diameters and albedos fall within $\pm \sim 20\%$ and $\pm \sim 40\%$, 1-sigma, respectively, of those measured by these alternate techniques. NEOWISE continues to preferentially discover near-Earth objects which are large (> 100 m), and have low albedos.

1. Introduction

Observing asteroids at infrared wavelengths is an effective method for calculating diameters for large numbers of asteroids. Since asteroid albedos can vary by approximately an order of magnitude, sizes estimated from reflected visible light fluxes alone have large uncertainties. Combining diameters calculated from infrared fluxes with visible magnitudes yields albedo measurements. Together, diameter and albedo measurements are basic physical characterizations that enable further investigations, including studies of asteroid families (Masiero et al. 2013; Walsh et al. 2013; Carruba et al. 2013; Milani et al. 2014; Masiero et al. 2015a,b) and size-frequency distributions (Zellner 1979; Gradie & Tedesco 1982; Tedesco et al. 2002; Bus & Binzel 2002; Mainzer et al. 2011b; Grav et al. 2012a, 2011; Bauer et al. 2013).

We present diameters and albedos of asteroids from the second year of the NEOWISE mission following the reactivation of the spacecraft from hibernation in late 2013. Diameters and albedos of asteroids from the first year of the NEOWISE mission following reactivation are given in Nugent et al. (2015). NEOWISE is a space-based infrared telescope that obtains an image of the sky every eleven seconds simultaneously in two bands, W1 (3.4 μm) and W2 (4.6 μm). From its sun-synchronous orbit around Earth, NEOWISE observes the entire static sky every six months. The original mission, WISE, is described in detail in Wright et al. (2010), and the NEOWISE enhancement to the mission is described in Mainzer et al. (2011a). After successfully completing its prime mission in 2011, the WISE spacecraft was placed into hibernation for 32 months before being reactivated and renamed NEOWISE in late 2013. The NEOWISE reactivation mission is described in Mainzer et al. (2014a).

The goals of the NEOWISE mission are to discover, track, and characterize minor planets. Images and extracted source lists from all phases of the WISE and NEOWISE missions have been delivered to the public via the Infrared Science Archive (Cutri et al. 2012, 2015), NASA’s designated archive for infrared astronomical data.

During the initial portion of the mission, NEOWISE employed four channels; 3.4, 4.6, 12, and 22 μm . The longest two wavelength channels required cooling to < 8 K using a dual-stage solid hydrogen cryostat. Diameters and albedos for a variety of small body populations were calculated using this fully cryogenic portion of the mission (see Table 1). As the cryogen was depleted, the 12 and 22 μm channels became inoperative; after this, the mission continued for several months using only its 3.4 and 4.6 μm channels. A summary of near-Earth asteroid (NEAs) and main belt asteroid (MBA) albedos and diameters calculated during various phases of the mission is given in Table 2. These measurements have also been submitted to NASA’s Planetary Data System. Thermal model calibration results, including comparison of cryogenic WISE/NEOWISE-derived diameters to other

observations, are given in Mainzer et al. (2011c,d).

This second year of data also provides multi-epoch observational data of uniform quality that can be used to better constrain the sizes, shapes, rotation state and thermophysical properties of the 9,092 asteroids in the reactivation Year 2 sample.

We present preliminary diameters and albedos calculated from NEOWISE Year 2 Reactivation mission observations, which spanned 13 December 2014 to 13 December 2015. Diameters and albedos calculated from NEOWISE Year 2 Reactivation mission observations will be submitted to the Planetary Data System.

2. Discoveries and follow-up

NEOWISE discovered 198 near-Earth asteroids and comets during Years 1 and 2 of the Reactivation mission. In addition to observing 175 NEAs that had not had diameters measured previously from NEOWISE data, the Year 2 Reactivation mission obtained thermal infrared observations at additional epochs for 32 NEAs. NEOWISE typically observes asteroids $\sim 10 - 12$ times over $\sim 1 - 1.5$ days, and requires a minimum of 5 detections of a discovery candidate for submission to the Minor Planet Center (MPC).

NEOWISE observes with a fixed observing cadence, and additional follow up observations are usually necessary to confirm that new minor planet candidates have been discovered. Since NEOWISE cannot perform targeted follow up on its own, these observations must be made by ground-based observers. Given that near-Earth objects (NEOs) are of a population of special interest, NEOWISE candidate NEOs are listed on the MPC Near-Earth Object Confirmation Page (NEOCP) to facilitate follow up. NEOWISE regularly relies on many ground-based observers for follow up, including Spacewatch, observers at the Institute for Astronomy at the University of Hawaii, the Las Cumbres Observatory Global telescope Network (LCOGT), the Magdalena Ridge Observatory, the

Table 1. Diameters and albedos for various small body populations, calculated from fully cryogenic (3.4, 4.6, 12 and 22 μm bands) NEOWISE mission data.

Population	Associated reference
Near-Earth asteroids	Mainzer et al. (2011b), Mainzer et al. (2014b)
Main belt asteroids	Masiero et al. (2011)
Active main belt objects	Bauer et al. (2012b)
Trojans	Grav et al. (2012b)
Hildas	Grav et al. (2012a)
Irregular satellites	Grav et al. (2015)
Centaurs	Bauer et al. (2013)
Comets	Bauer et al. (2011, 2012a, 2015),

Table 2. Previously published papers containing NEA and MBA diameters and albedos calculated from NEOWISE mission data.

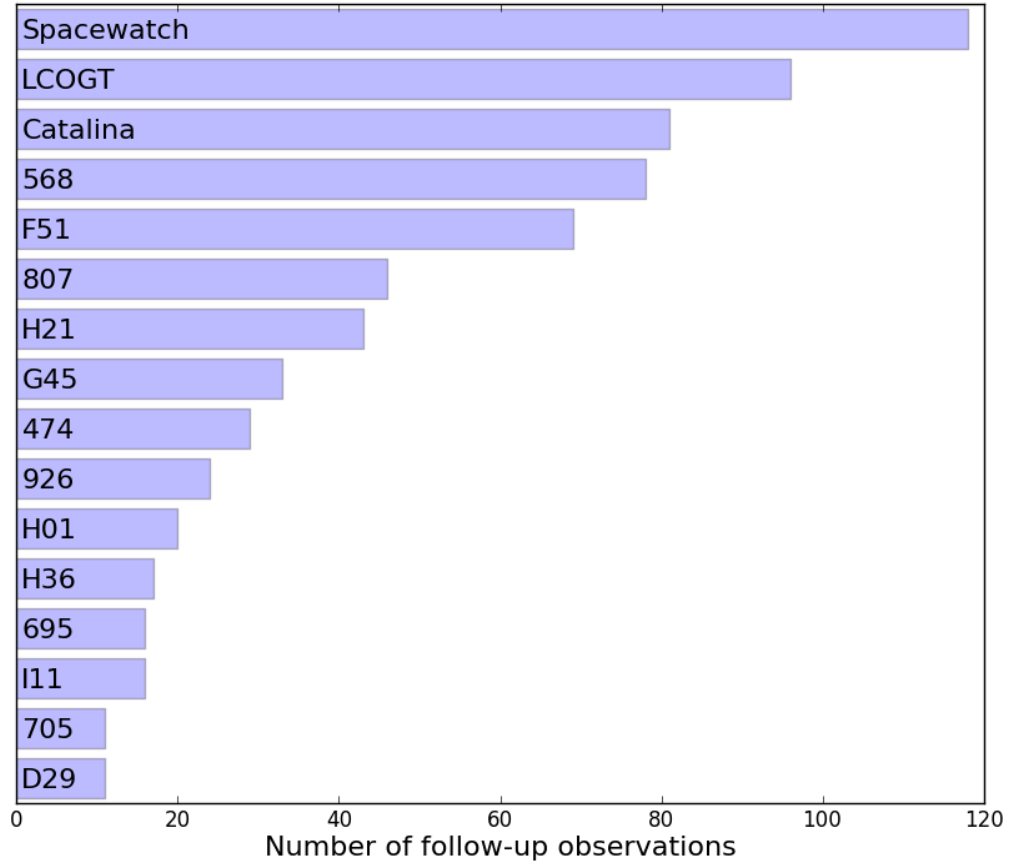
Mission Phase	Detection bands (μm)	Reference for NEAs	Reference for MBAs
Fully cryogenic	3.4, 4.6, 12, 22	Mainzer et al. (2011b),	Masiero et al. (2011),
		Mainzer et al. (2014b)	Masiero et al. (2014)
3-Band and Post cryogenic	3.4, 4.6, (some 12)	Mainzer et al. (2012a)	Masiero et al. (2012)
Year 1 of reactivation	3.4, 4.6	Nugent et al. (2015)	Nugent et al. (2015)

Mt. John Observatory, and a number of amateur observers across the globe to coordinate follow up of particular objects. The NEOWISE team was granted eight hours each semester of Target of Opportunity observing time on Gemini Observatory’s Gemini South telescope (Hook et al. 2004) as well as time on the Blanco 4m/Dark Energy Camera (DECam; Flaugher et al. 2015), and was granted Co-I status on the LCOGT NEO follow up program. Access to these facilities is vital for following up of discoveries deep in the Southern Hemisphere.

Figure 1 is a histogram of the observatories and campaigns that contributed the majority of follow observations occurring immediately after NEOWISE reported candidate observations, including Spacewatch (McMillan 2007), with over 100 follow-up observations, the Las Cumbres Observatory Global Telescope Network (Brown et al. 2013), and the Catalina Sky Survey (Christensen et al. 2015). Observers on Mauna Kea using the University of Hawaii 2.2m telescope and the Canada-France-Hawaii Telescope’s Megacam imager repeatedly obtained follow-up of objects under challenging observing conditions (e.g. Tholen et al. 2014). The Mt John University Observatory (observatory code 474) obtained valuable observations of 2015 OA₂₂. NEOWISE discovered this object at -70° declination, and ephemerides showed it was moving further South. The Mt John University Observatory was able to track the object to -78° declination, confirming the discovery.

NEOWISE submitted several candidate objects to the MPC that were not placed on the NEOCP based on an initial orbit determination that indicated they were not NEOs. These did not receive targeted follow-up. Fifty-seven non-NEO NEOWISE discoveries made during the Reactivation mission do not have associated orbits. Additionally, there were eight objects (main belt asteroids, Hungarias, and Mars-crossers) detected solely by NEOWISE that were given provisional designations by the MPC; all of these objects have poorly determined orbits. Without well-determined orbits, distance at observing time cannot be computed accurately, and therefore diameters were not determined for these

Fig. 1.— NEOWISE relies on ground-based observatories to perform targeted follow up of candidate NEO discoveries. This histogram shows numbers of follow-up observations taken by different groups (listed by their MPC observatory codes) for NEOWISE discoveries during Year 1 and Year 2 of the Reactivation mission.



objects.

2.1. Comets

The NEOWISE Reactivation mission has detected over 100 comets, including eight discoveries (four of which were made after the end of the second year of observations). The NEOWISE spacecraft is sensitive to the presence of coma dust, as well as the CO-line ($4.67\text{ }\mu\text{m}$) and CO₂-line ($4.23\text{ }\mu\text{m}$) emission from comet comae from gas species which are obscured or completely blocked by Earth's atmosphere (Figure 2). Analysis of the excess emission at $3.4\text{ }\mu\text{m}$ by Bauer et al. (2015) provided CO+CO₂ production rates and limits of the first four comets discovered by the NEOWISE Reactivation mission.

The infrared wavelengths provide a thermal emission and reflected light dust signal that can characterize a unique regime of dust particle sizes through analysis of the dust coma morphologies (Kramer et al. 2015). The NEOWISE multi-epoch observations of many of the comets detected so far provide characterization of long-term cometary behavior regarding these aspects of dust and gas emission. The gas and dust properties of the Reactivation Year 1 and 2 survey comet sample will be described in a later work.

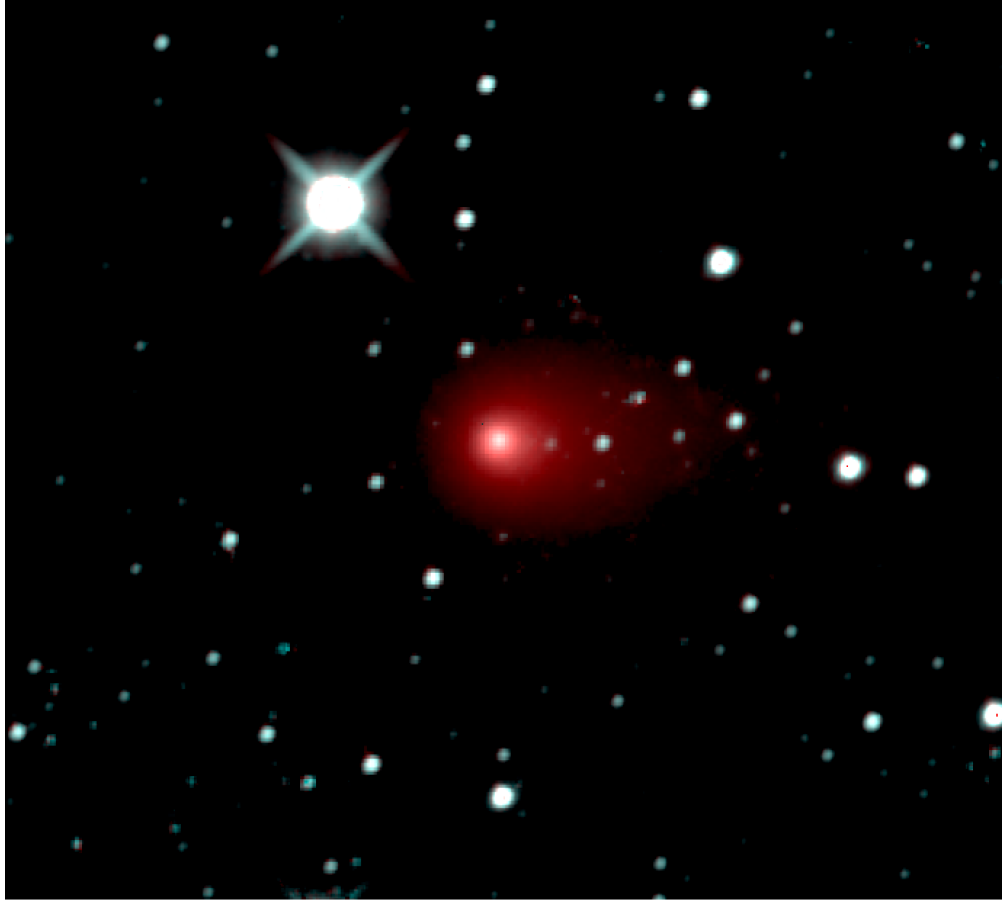
3. Methods

3.1. Extraction of Detections

The methodology for extracting detections of minor planets from the NEOWISE source lists, as well as methods of diameter and albedo computation follows the description in Nugent et al. (2015), with the one exception described in Section 3.2. As was done in that work, the NEOWISE source lists were searched using the positions and times reported for each minor planet in the MPC's archival files NumObs.txt and UnnObs.txt¹. NEOWISE reports detections to the MPC three times a week. By querying the MPC archive after

¹<http://www.minorplanetcenter.net/iau/ECS/MPCAT-OBS/MPCAT-OBS.html>

Fig. 2.— Comet C/2013 US₁₀ (Catalina) as seen by NEOWISE on August 28, 2015. The 2-color image maps the 3.4 μm band to the cyan, and the 4.6 μm band to the red. The image is a quarter-degree on a side and is oriented approximately with North down and East is to the left. The red appearance suggests the comet may have significant CO or CO₂ emission.



the conclusion of Year 2 operations, we restrict our analysis to those detections of minor planets that were reported to and confirmed by the MPC.

These detections were converted into IRSA Catalog Query Engine format², and were used to query the NEOWISE-R Single Exposure Level 1b (L1b) Source Table, which is served by the NASA/IPAC Infrared Science Archive (IRSA). The NEOWISE Reactivation

²<http://irsa.ipac.caltech.edu/applications/Gator/GatorAid/irsa/QuickGuidetoGator.htm>

data are described in detail in the NEOWISE Reactivation Explanatory Supplement (Cutri et al. 2015), which was updated in March 2016 to include single-exposure images and extracted source products from Reactivation Year 2. The Single Exposure (L1b) Source table was queried to find sources within 2 arcseconds of the reported position in the MPC files. For this query, detection time is constrained to be within two seconds of the reported time. The resulting table is a list of all sources corresponding to reported MPC detections from single exposures, with associated MPC designations for each detection.

Several steps are taken to prevent confusion of small body detections with fixed background sources such as stars and galaxies. We reference the WISE All-Sky Source Catalog, which is derived from a co-add of multiple exposures, covering the sky. This is a significantly deeper image than the individual L1b images, and pixel outlier rejection suppresses moving solar system objects. Therefore, it is useful for identifying fixed sources in the L1b images. The WISE Moving Object Pipeline System (WMOPS), which identifies moving objects in the NEOWISE images, compares single-exposure detections to reference images before any detections are submitted to the MPC. However, as an additional precaution, we also compare the single-exposure detection list to the All-Sky Catalog. Any single-exposure detections found to be within 6.5 arcseconds (the size of the 3.4 and 4.6 μm NEOWISE point-spread function) of a WISE All-Sky Source Catalog source with $\text{SNR} \geq 3$ were removed.

The resulting asteroid detection table was then stripped of measurements with associated poor quality flags. Each NEOWISE detection is graded for quality, as described in Cutri et al. (2015). Detections with “*ph_qual*” values of “A”, “B”, or “C” were accepted, this photometric quality grade ensures that the source was detected in the band with a flux signal-to-noise ratio < 2 . Additionally, detections must have “*cc_flags*” values of “0” or “p”, indicating that either the source was unaffected by known artifacts (“0”), or perhaps is impacted by a latent image left by a bright source (“p”). The value of “p” is conservative;

it indicates the source is likely unaffected by a latent image, but possibly may be slightly contaminated. Finally, only frames graded “*qual_frame*=“10” or highest quality by the quality assurance process were used.

The WISE Science Data System pipeline profile-fitting magnitudes are used for each band (Cutri et al. 2015). A minimum of three detections with measurement uncertainties $\sigma_{mag} \leq 0.25$ mag were required for thermal fits. Saturated detections, with a W1 magnitude ≤ 8.0 or a W2 magnitude ≤ 7.0 , were discarded. The photometric measurements used for each asteroid are listed in Table 3.

3.2. H and G values

For each diameter, a corresponding albedo is also calculated, using an absolute visual magnitude H and IAU phase slope parameter G (Bowell et al. 1989). Therefore, the accuracy of albedos calculated from diameter measurements depends on the accuracy H and G values. The MPC provides H and G values as part of its catalog service; however, the default catalog values may be affected by various systematic effects (Vereš et al. 2015; Williams 2012). Known issues include values calculated from observations submitted with uncertain photometric calibrations and a bias towards discovering asteroids when their longest axis faces Earth (Jedicke et al. 2002).

Corrected or newly-derived H and G values have been published by Warner et al. (2009); Pravec et al. (2012); Williams (2012) and Vereš et al. (2015). The largest of these H and G datasets is from Williams (2012) with ~ 337000 numbered asteroids, and Vereš et al. (2015) with ~ 250000 objects observed by Pan-STARRS PS1. The Williams (2012) dataset is slated to be incorporated into the MPC catalog (G. Williams, personal communication, May 2nd 2016). For this reason, and because it is more extensive, we used these corrected H and G values in this work when they were available for the asteroids in our sample. This

is a departure from the methods in Nugent et al. (2015), which employed MPC database H and G values as no large replacement dataset was available at that time. Unless specified otherwise, G is assumed to be 0.15 ± 0.1 mag, and the error in H is assumed to be ± 0.3 mag.

3.3. Diameter and albedo calculations

The effective diameter d of each asteroid and geometric optical albedo p_v were then calculated from the resulting verified, high-quality minor planet measurements using the Near-Earth Asteroid Thermal Model (NEATM; Harris 1998). The implementation used in this work is detailed in Mainzer et al. (2011c). It assumes a spherical object with no rotation, no nightside emission, and a temperature distribution given by:

$$T(\theta) = T_{max} \cos^{1/4}(\theta) \quad \text{for } 0 \leq \theta \leq \pi/2 \quad (1)$$

where θ is the angular distance from the sub-solar point. T_{max} is the sub-solar temperature, defined as:

$$T_{max} = \left(\frac{(1 - A)S}{\eta \epsilon \sigma} \right)^{1/4} \quad (2)$$

where A is the bolometric Bond albedo, S is the solar flux at the asteroid, η is the beaming parameter, ϵ is the emissivity, and σ is the Stefan-Boltzmann constant. The beaming parameter η adjusts the temperature distribution, and variation of η can be due to non-spherical shapes, rotation rates, spin pole orientation with respect to observer, surface thermal inertia, phase effects, etc.

After a best-fit diameter is found, twenty-five Monte Carlo trials were run to evaluate the errors introduced by the uncertainty in the flux measurements. The corresponding uncertainties in diameter and albedo, along with the H and G values used as inputs to the thermal model, are reported in Tables 4 and 5.

The NEOWISE survey cadence observes each object over ~ 1.5 days on average, and sometimes re-observes an object ~ 3 to ~ 6 months later at a different distance and viewing geometry. These separate epochs, defined as observations separated by > 10 days, the typical amount of time for viewing geometry of NEOs to change significantly, were fit separately.

NEAs were treated differently than Mars-crossing and main belt asteroids, because of the different characteristics of the populations and different phase angles as demonstrated in Mainzer et al. (2011b) and Masiero et al. (2011). In most cases, NEAs were fit with $\eta = 1.4 \pm 0.5$. If both bands were thermally dominated, a beaming parameter was fit. A ratio of $p_{IR}/p_V = 1.6 \pm 1.0$ was assumed for NEAs. Mars-crossing and main belt asteroids were fit with $\eta = 0.95 \pm 0.2$, and the ratio of p_{IR}/p_V was taken to be 1.5 ± 0.1 in most cases. These assumptions were necessary because if only one thermally dominated band is available, a beaming parameter cannot be fit; similarly, with only the 3.4 and 4.6 μm bands, we cannot fit p_{IR} because there is not enough information to constrain it.

As noted in Tables 4 and 5, some objects were fit with alternative beaming parameters and p_{IR}/p_V ratios. In rare cases the standard assumption of $\eta = 1.4 \pm 0.5$ and $\eta = 0.95 \pm 0.2$ for NEAs and MBAs, respectively, lead to poor fits. Poor fits are indicated by $abs(H_{observed} - H_{modeled}) > 0.5$ or unphysical values of p_V , generally taken to be $p_V < \sim 0.02$, $p_V > \sim 0.6$). In cases where a poor fit is obtained, we use the constraints on H magnitude errors and physical limits on albedo to exclude unphysical results, and rule out certain beaming and p_{IR}/p_V values. A series of broadly-spaced beaming values (in increments of 0.2) and p_{IR}/p_V ratios (in increments of 0.5) were tried; in these few cases, the associated errors were increased. These spacings were chosen so that in most cases only a single pair of beaming and p_{IR}/p_V ratios would produce a good fit.

NEATM is only effective if at least one of the wavelength bands employed is dominated by thermal emission. Therefore, any object found to have $< 75\%$ thermally emitted light

(generally the cooler outer main belt objects) in both bands was removed from the results. This determination is made after an initial fit to the object is completed and estimates of thermally emitted and reflected light can be computed.

4. Results

Thermal fit results for NEAs are presented in Table 4; Table 5 contains the fit results for Mars-crossing and main belt asteroids. When objects were observed at multiple epochs, a measurement of diameter and albedo is given for each epochs.

Some asteroids have diameters and albedos calculated from earlier NEOWISE measurements (Mainzer et al. 2011b; Masiero et al. 2011; Mainzer et al. 2012a; Masiero et al. 2012; Nugent et al. 2015). Figure 3 is a histogram of the diameters and albedos for these objects measured from Reactivation Year 2 data and previous work. This figure also compares the results of the corrected H and G values from Williams (2012). Although distributions of diameter and albedo for this work are comparable to previous NEOWISE results, the incorporation of the revised H and G values does shift the albedo distribution towards slightly lower values. The implementation of the Williams (2012) H and G values did not change the diameters of the ensemble of NEAs or other asteroids in a statistically significant way (see Figure 3).

When possible, diameters calculated from this work were compared to diameters calculated by independent methods (Figure 4). Twenty-three objects have diameters calculated via stellar occultations (Shevchenko & Tedesco 2006), eleven have radar-derived shapes (Benner et al. 2015), and two, (951) Gaspra and (253) Mathilde, were observed by spacecraft and had shape and size determined from resulting images (Thomas et al. 1994, 1999). These comparison cases were not preselected on light curve amplitude. When three-dimensional shapes were known, comparison was made to the average of

the length of each axis. As illustrated in Figure 4, a Gaussian fit to a histogram of $(D_{NEOWISE} - D_{reference})/D_{NEOWISE}$ gives $\sigma = 20\%$, and a Gaussian fit to a histogram of $(p_{v-NEOWISE} - p_{v-reference})/p_{v-NEOWISE}$ gives $\sigma = 40\%$.

We report the Gaussian-fit $1 - \sigma$ uncertainty of 20% on diameter, and 40% on albedo, based on the comparison to diameter measurements made with other techniques known to produce highly accurate diameters. This encompasses the systematic uncertainties in the comparison measurements (radar, stellar occultation, and spacecraft measurements), the range of ways that actual objects do not precisely match with the assumptions of NEATM, as well as the color corrections derived for the WISE filters (Wright et al. 2010).

The diameters and albedos of NEOWISE Reactivation discoveries are compared with the diameters and albedos of objects detected during Reactivation operations in Figure 5. NEOWISE continues to discover large objects (> 100 m), as well as low-albedo objects.

4.1. Potentially Hazardous Asteroids

Potentially Hazardous Asteroids (PHAs) have been defined as objects with $H \leq 22.0$ mag and a Minimum Orbit Intersection Distance (MOID) of 0.05 AU. The MOID is a measurement of the smallest distance between two orbits (SitarSKI 1968; Gronchi 2005). Since many NEAs do not have measured diameters, the H limit was used as a proxy for size. An object with $p_V = \sim 0.14$ and $H = 22.0$ mag corresponds to an object ~ 140 m in diameter.

Using the PHA definition as defined by H limit, five NEOWISE Reactivation Year 2 discoveries are considered PHAs. However, eight NEOWISE Reactivation Year 2 discoveries are larger than 140 m in diameter and have a $\text{MOID} \leq 0.05$ AU, and therefore should be classified as PHAs. With the availability of more diameter measurements of NEAs from NEOWISE, the Spitzer Space Telescope (Trilling et al. 2010), and ground-based facilities,

sizes should be taken into consideration when designating PHAs as suggested in Mainzer et al. (2012b). The fraction of PHAs within the NEOWISE NEA discoveries remains virtually constant across Year 1 and Year 2 of the Reactivation mission, and is nearly a factor of three higher than ground-based surveys³.

4.2. NHATS

The Near-Earth Object Human Space Flight Accessible Targets Study (NHATS, Barbee et al. 2013) aims to identify the asteroids that would be most accessible to a crewed mission to an asteroid⁴. NHATS-compliant targets must pass a series of restrictions, including Earth departure dates before 31 Dec 2040, total mission $\Delta V \leq 12 \text{ km s}^{-1}$, and a minimum NEA stay time of 8 days. Many of these objects do not have measured physical properties. The NEOWISE Year 2 Reactivation mission measured diameters and albedos for eight objects (Table 6). Two, (35107) 1991 VH and (363505) 2003 UC₂₀, were observed during Reactivation Year 1.

5. Conclusion

NEOWISE continues its mission to discover, track, and characterize minor planets. This release of diameters and albedos for 9,092 asteroids measured using NEOWISE Year 2 observations increases the total number of asteroids with measured diameters and albedos by 1,440, enabling further studies of NEAs and other asteroids by the scientific community and provides multi-epoch infrared observations that support more detailed thermophysical modeling studies. Comparison to diameters measured by other methods shows that

³<http://neo.jpl.nasa.gov/stats/>

⁴<http://neo.jpl.nasa.gov/nhats/>

measured diameters continue to be accurate to $\sim 20 + \%$ during the Year 2 Reactivation mission. NEOWISE continues to preferentially discover large ($> 100\text{m}$), low-albedo NEOs.

6. Acknowledgments

The authors thank the reviewer, Valerio Carruba, for his careful review that improved the quality of this manuscript.

This publication makes use of data products from the Wide-field Infrared Survey Explorer, which is a joint project of the University of California, Los Angeles, and JPL/California Institute of Technology, funded by NASA. This publication also makes use of data products from NEOWISE, which is a project of the JPL/California Institute of Technology, funded by the Planetary Science Division of NASA. The JPL High-Performance Computing Facility used for our simulations is supported by the JPL Office of the CIO.

This research has made use of the NASA/ IPAC Infrared Science Archive, which is operated by the Jet Propulsion Laboratory, California Institute of Technology, under contract with the National Aeronautics and Space Administration.

This project used data obtained with the Dark Energy Camera (DECam), which was constructed by the Dark Energy Survey (DES) collaboration. Funding for the DES Projects has been provided by the U.S. Department of Energy, the U.S. National Science Foundation, the Ministry of Science and Education of Spain, the Science and Technology Facilities Council of the United Kingdom, the Higher Education Funding Council for England, the National Center for Supercomputing Applications at the University of Illinois at Urbana-Champaign, the Kavli Institute of Cosmological Physics at the University of Chicago, the Center for Cosmology and Astro-Particle Physics at the Ohio State University, the Mitchell Institute for Fundamental Physics and Astronomy at Texas A&M University, Financiadora de Estudos e Projetos, Fundação Carlos Chagas Filho de Amparo à Pesquisa do Estado do

Rio de Janeiro, Conselho Nacional de Desenvolvimento Científico e Tecnológico and the Ministério da Ciência, Tecnologia e Inovação, the Deutsche Forschungsgemeinschaft, and the Collaborating Institutions in the Dark Energy Survey. The Collaborating Institutions are Argonne National Laboratory, the University of California at Santa Cruz, the University of Cambridge, Centro de Investigaciones Enérgéticas, Medioambientales y Tecnológicas-Madrid, the University of Chicago, University College London, the DES-Brazil Consortium, the University of Edinburgh, the Eidgenössische Technische Hochschule (ETH) Zürich, Fermi National Accelerator Laboratory, the University of Illinois at Urbana-Champaign, the Institut de Ciències de l'Espai (IEEC/CSIC), the Institut de Física d'Altes Energies, Lawrence Berkeley National Laboratory, the Ludwig-Maximilians Universität München and the associated Excellence Cluster Universe, the University of Michigan, the National Optical Astronomy Observatory, the University of Nottingham, the Ohio State University, the University of Pennsylvania, the University of Portsmouth, SLAC National Accelerator Laboratory, Stanford University, the University of Sussex, and Texas A&M University.

This work makes use of observations from the LCOGT network.

The authors wish to thank G. Williams, for providing the corrected H and G values from his dissertation used in this work.

This publication makes use of observations obtained at the Gemini Observatory, which is operated by the Association of Universities for Research in Astronomy, Inc., under a cooperative agreement with the NSF on behalf of the Gemini partnership: the National Science Foundation (United States), the National Research Council (Canada), CONICYT (Chile), Ministerio de Ciencia, Tecnología e Innovación Productiva (Argentina), and Ministério da Ciência, Tecnologia e Inovação (Brazil). Observing Program IDs: GS-2015A-LP-3, GS-2015B-LP-3.

Fig. 3.— Comparison between asteroid diameters (top) and albedos (bottom) measured in this work with H and G values from the MPC (blue), diameters for the same objects measured in this work with revised H and G values from Williams (2012) (black), and diameters for the same objects measured using previous NEOWISE measurements, which employed H and G values from the MPC (green). The bimodal structure of the albedo distribution is due to the populations of bright S-type ($p_V = 0.25$) and dark C-type ($p_V = 0.06$) objects in the main belt.

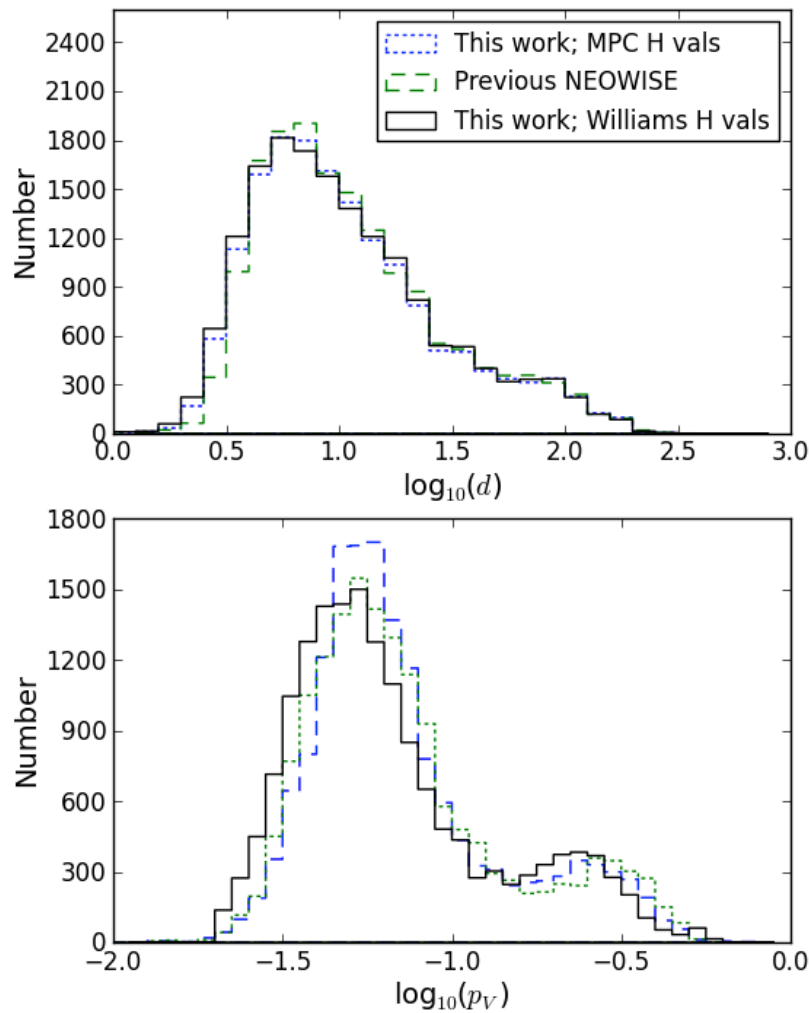


Fig. 4.— Top: Comparison of diameters and albedos derived via radar, stellar occultations, and spacecraft flybys to the values calculated in this paper. The dashed red line shows a 1:1 relation. Bottom: Histograms of the fractional differences between the NEOWISE diameters ($\% \Delta d$, left) and albedos ($\% \Delta p_V$, right) and those derived from other methods. Dashed red line is best-fit Gaussian, with the fitted σ given in the legends.

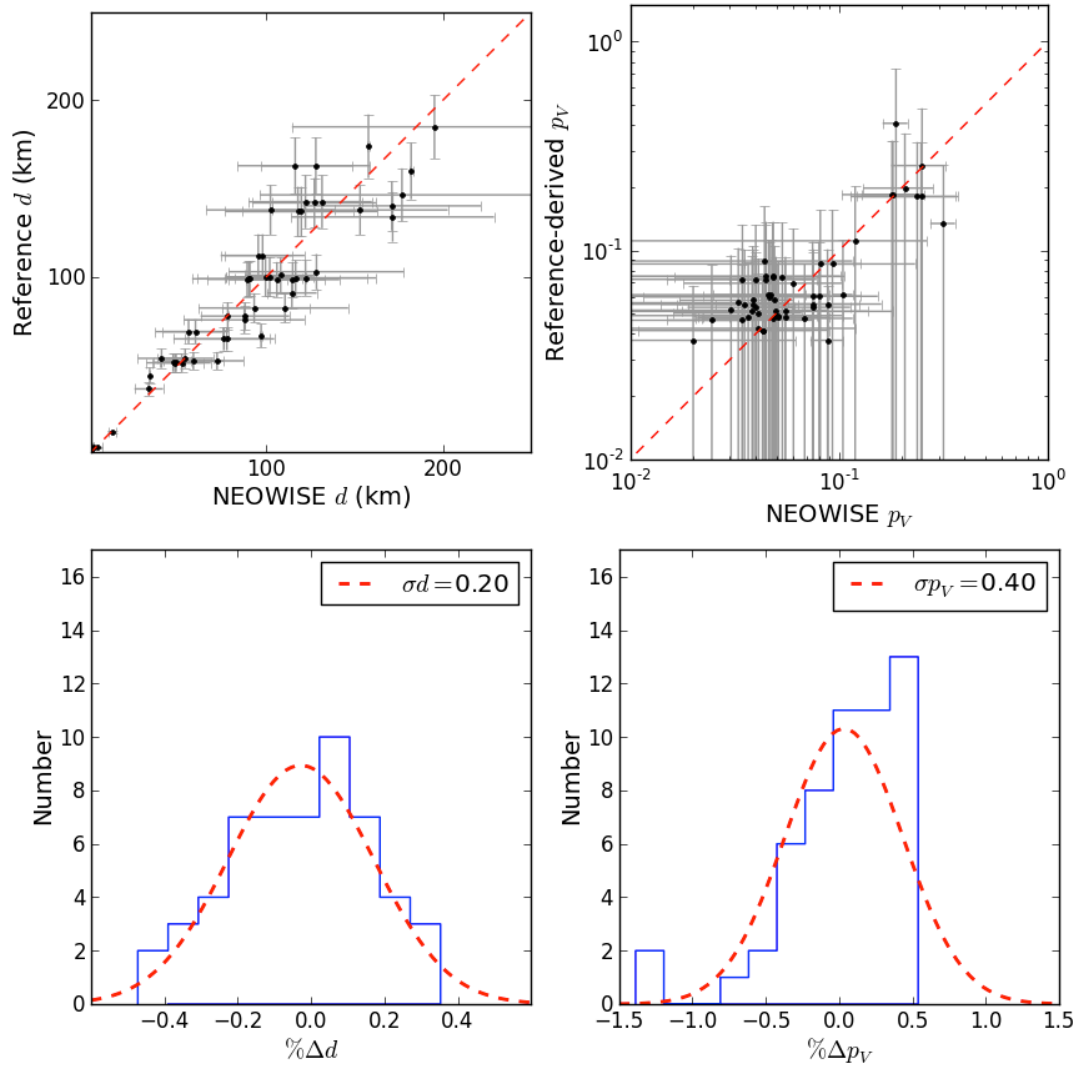
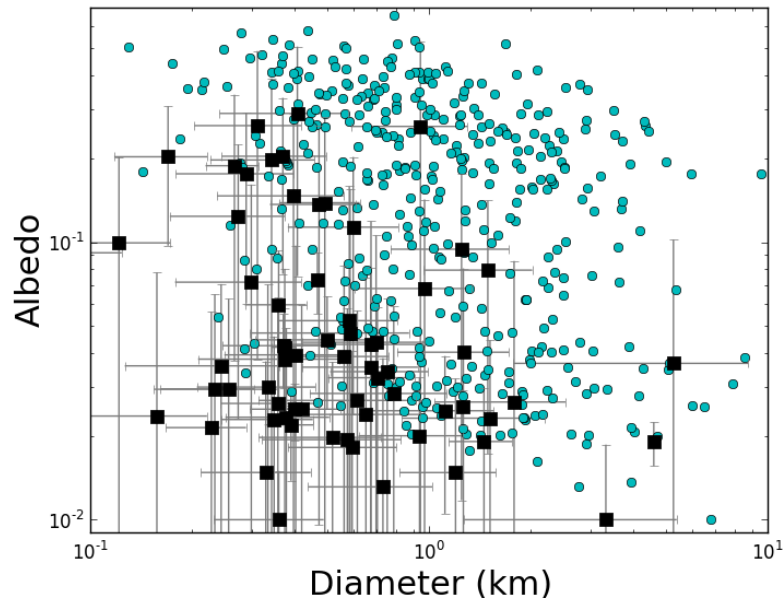


Fig. 5.— Diameters and albedos from NEOWISE measurements of previously known NEAs (teal circles) and NEOWISE NEA discoveries (black squares) made during years 1 and 2 of the Reactivation. NEOWISE continues to detect large objects > 100 m, and many discoveries are dark. Error bars on previously known objects were omitted for clarity.



REFERENCES

- Barbee, B. W., Abell, P. A., Adamo, D. R., et al. 2013, 2013 IAA Planetary Defense Conference Proceedings
- Bauer, J. M., Grav, T., Blauvelt, E., et al. 2013, *The Astrophysical Journal*, 773, 22
- Bauer, J. M., Kramer, E., Mainzer, A. K., et al. 2012a, *The Astrophysical Journal*, 758, 18
- Bauer, J. M., Mainzer, A. K., Grav, T., et al. 2012b, *The Astrophysical Journal*, 747, 49
- Bauer, J. M., Stevenson, R., Kramer, E., et al. 2015, *The Astrophysical Journal*, 814, 85
- Bauer, J. M., Walker, R. G., Mainzer, A. K., et al. 2011, *The Astrophysical Journal*, 738, 171
- Benner, L., Busch, M. B., Giorgini, J. D., Taylor, P. A., & Margot, J. L. 2015, Asteroids IV
- Bowell, E., Hapke, B., Domingue, D., et al. 1989, in *Asteroids II*, 524–556
- Brown, T. M., Baliber, N., Bianco, F. B., et al. 2013, *Publications of the Astronomical Society of the Pacific*, 125, 1031
- Bus, S. J. & Binzel, R. P. 2002, *Icarus*, 158, 146
- Carruba, V., Domingos, R. C., Nesvorný, D., et al. 2013, *Monthly Notices of the Royal Astronomical Society*, 433, 2075
- Christensen, E. J., Carson Fuls, D., Gibbs, A. R., et al. 2015, in *AAS/Division for Planetary Sciences Meeting Abstracts*, Vol. 47, *AAS/Division for Planetary Sciences Meeting Abstracts*, 308.19
- Cutri, R. M., Mainzer, A., Conrow, T., et al. 2015, 1, explanatory Supplement to the NEOWISE Data Release Products,
<http://wise2.ipac.caltech.edu/docs/release/neowise/expsup>

- Cutri, R. M., Wright, E. L., Conrow, T., et al. 2012, 1,
http://wise2.ipac.caltech.edu/docs/release/allsky/expsup/sec8_1.html
- Flaugher, B., Diehl, H. T., Honscheid, K., et al. 2015, AJ, 150, 150
- Gradie, J. & Tedesco, E. 1982, Science, 216, 1405
- Grav, T., Mainzer, A. K., Bauer, J., et al. 2012a, The Astrophysical Journal, 744, 197
- . 2011, The Astrophysical Journal, 742, 40
- Grav, T., Mainzer, A. K., Bauer, J. M., Masiero, J. R., & Nugent, C. R. 2012b, The Astrophysical Journal, 759, 49
- Grav, T. et al. 2015, The Astrophysical Journal, 809, 3
- Gronchi, G. F. 2005, Celestial Mechanics and Dynamical Astronomy, 93, 295
- Harris, A. W. 1998, Icarus, 131, 291
- Hook, I. M., Jørgensen, I., Allington-Smith, J. R., et al. 2004, The Publications of the Astronomical Society of the Pacific, 116, 425
- Jedicke, R., Larsen, J., & Spahr, T. 2002, Observational Selection Effects in Asteroid Surveys, ed. W. F. Bottke, Jr., A. Cellino, P. Paolicchi, & R. P. Binzel, 71–87
- Kramer, E. A., Bauer, J. M., Fernández, Y. R., et al. 2015, in AAS/Division for Planetary Sciences Meeting Abstracts, Vol. 47, AAS/Division for Planetary Sciences Meeting Abstracts, 506.09
- Mainzer, A., Bauer, J., Cutri, R. M., et al. 2014a, The Astrophysical Journal, 792, 30
- Mainzer, A., Bauer, J., Grav, T., et al. 2011a, The Astrophysical Journal, 731, 53
- . 2014b, The Astrophysical Journal, 784, 110

- Mainzer, A., Grav, T., Bauer, J., et al. 2011b, *The Astrophysical Journal*, 743, 156
- Mainzer, A., Grav, T., Masiero, J., et al. 2012a, *The Astrophysical Journal Letters*, 760, L12
- . 2012b, *The Astrophysical Journal*, 752, 110
- . 2011c, *The Astronomical Journal*, 736, 100
- . 2011d, *The Astrophysical Journal Letters*, 737, L9
- Masiero, J., DeMeo, F., Kasuga, T., & Parker, A. H. 2015a, ArXiv e-prints
- Masiero, J. R., Grav, T., Mainzer, A. K., et al. 2014, *The Astrophysical Journal*, 791, 121
- Masiero, J. R., Mainzer, A. K., Bauer, J. M., et al. 2013, *The Astrophysical Journal*, 770, 7
- Masiero, J. R., Mainzer, A. K., Grav, T., et al. 2011, *The Astrophysical Journal*, 741, 68
- . 2012, *The Astrophysical Journal Letters*, 759, L8
- Masiero, J. R. et al. 2015b, *The Astrophysical Journal*, 809, 179
- McMillan, R. S. 2007, in IAU Symposium, Vol. 236, IAU Symposium, ed. G. B. Valsecchi, D. Vokrouhlický, & A. Milani, 329–340
- Milani, A., Cellino, A., Knežević, Z., et al. 2014, *Icarus*, 239, 46
- Nugent, C. R., Mainzer, A., Masiero, J., et al. 2015, *The Astrophysical Journal*, 814, 117
- Pravec, P., Harris, A. W., Kušnírák, P., Galád, A., & Hornoch, K. 2012, *Icarus*, 221, 365
- Shevchenko, V. G. & Tedesco, E. F. 2006, *Icarus*, 184, 211
- Sitarski, G. 1968, *Acta Astronomica*, 18, 171

- Tedesco, E. F., Noah, P. V., Noah, M., & Price, S. D. 2002, *The Astronomical Journal*, 123, 1056
- Tholen, D. J., Mainzer, A. K., Bauer, J. M., et al. 2014, *Minor Planet Electronic Circulars*, 145
- Thomas, P. C., Veverka, J., Bell, J. F., et al. 1999, *Icarus*, 140, 17
- Thomas, P. C., Veverka, J., Simonelli, D., et al. 1994, *Icarus*, 107, 23
- Trilling, D. E., Mueller, M., Hora, J. L., et al. 2010, *The Astronomical Journal*, 140, 770
- Vereš, P., Jedicke, R., Fitzsimmons, A., et al. 2015, *Icarus*, 261, 34
- Walsh, K. J., Delbó, M., Bottke, W. F., Vokrouhlický, D., & Lauretta, D. S. 2013, *Icarus*, 225, 283
- Warner, B. D., Harris, A. W., & Pravec, P. 2009, *Icarus*, 202, 134
- Williams, G. V. 2012, PhD thesis, Open University UK
- Wright, E. L., Eisenhardt, P. R. M., Mainzer, A. K., et al. 2010, *The Astronomical Journal*, 140, 1868
- Zellner, B. 1979, Asteroid taxonomy and the distribution of the compositional types, ed. T. Gehrels (The University of Arizona Press), 783–806

Table 3. NEOWISE magnitudes for the NEAs modeled in this paper. Listed are MPC-packed name, the time of the observation in modified Julian date (MJD), and the magnitude in the $3.4\mu\text{m}$ (W1) and $4.6\mu\text{m}$ bands (W2). Non-detections at a particular wavelength represent 95% confidence limits (Cutri et al. 2012). Observations for the first two objects only are shown; the remainder are available in electronic format through the journal website.

Object	MJD	W1 (mag)	W2 (mag)
01580	57059.5362951	14.638 ± 0.074	11.338 ± 0.024
01580	57059.7989937	14.540 ± 0.068	11.339 ± 0.024
01580	57059.9304065	14.564 ± 0.076	11.274 ± 0.025
01580	57060.0618195	14.525 ± 0.084	11.290 ± 0.028
01580	57162.4156505	11.563 ± 0.017	8.478 ± 0.015
01580	57162.4812294	11.507 ± 0.017	8.436 ± 0.012
01580	57162.5468084	11.586 ± 0.018	8.497 ± 0.013
01580	57162.6780938	11.527 ± 0.019	8.436 ± 0.014
01580	57162.8092518	11.449 ± 0.017	8.388 ± 0.013
01580	57163.2684322	11.724 ± 0.018	8.624 ± 0.015
01580	57163.5308722	11.825 ± 0.021	8.695 ± 0.014
01580	57163.5309995	11.836 ± 0.021	8.443 ± 0.014
01580	57163.7933154	11.879 ± 0.019	8.803 ± 0.013
01580	57163.9246007	11.808 ± 0.021	8.737 ± 0.013
01580	57164.1213378	11.317 ± 0.017	8.222 ± 0.013
01580	57164.3837815	11.406 ± 0.021	8.286 ± 0.015
01580	57164.7772554	11.442 ± 0.021	8.373 ± 0.015
01580	57164.8429617	11.566 ± 0.021	8.512 ± 0.013
01580	57164.9741197	11.507 ± 0.019	8.381 ± 0.012
01580	57165.1052777	11.417 ± 0.020	8.371 ± 0.014
01580	57165.2364356	11.388 ± 0.026	8.330 ± 0.014
01580	57165.2365629	11.432 ± 0.021	8.316 ± 0.012
01580	57189.9632607	12.328 ± 0.023	9.224 ± 0.014
01580	57190.0288402	12.292 ± 0.023	9.209 ± 0.013
01580	57190.0944191	12.292 ± 0.026	9.204 ± 0.015
01580	57190.1601254	12.022 ± 0.028	8.925 ± 0.012
01580	57190.2257043	12.318 ± 0.028	9.243 ± 0.014
01580	57190.2912832	12.307 ± 0.022	9.198 ± 0.014
01580	57190.3568621	12.424 ± 0.025	9.268 ± 0.015
01620	57259.6667067	14.743 ± 0.082	12.908 ± 0.061
01620	57259.7979924	12.689 ± 0.104	12.701 ± 0.055
01620	57259.9291508	15.247 ± 0.130	13.368 ± 0.099

Table 3—Continued

Object	MJD	W1 (mag)	W2 (mag)
01620	57260.0603091	15.713 ± 0.177	13.865 ± 0.138
01620	57260.2570466	15.336 ± 0.134	13.066 ± 0.071
01620	57260.2571739	15.263 ± 0.125	13.355 ± 0.092
01620	57260.3227531	14.641 ± 0.075	12.867 ± 0.067
01620	57260.3883323	15.517 ± 0.150	13.546 ± 0.158
01620	57260.4539115	14.675 ± 0.079	12.747 ± 0.067
01620	57260.5850698	14.916 ± 0.091	13.053 ± 0.069
01620	57260.7818073	14.934 ± 0.108	12.796 ± 0.060
01620	57260.913093	15.390 ± 0.135	13.504 ± 0.114
01620	57261.1754097	15.203 ± 0.115	13.108 ± 0.070

Table 4. Measured diameters (d) and albedos (p_V) of near-Earth asteroids observed during the NEOWISE Year 2 mission. Asteroids may be identified by numbers, provisional designations, or via the MPC packed format. Magnitude H , slope parameter G , and beaming η used are given. The numbers of observations used in the $3.4\ \mu\text{m}$ (n_{W1}) and $4.6\ \mu\text{m}$ (n_{W2}) wavelengths are also reported, along with the amplitude of the $4.6\ \mu\text{m}$ light curve (W2 amp., in mag).

Object	Packed	H	G	d (km)	p_V	η	p_{IR}/p_V	W2 amp.	n_{W1}	n_{W2}
1580	01580	14.90	0.12	7.91 ± 0.08	0.03 ± 0.01	1.40 ± 0.00	2.31 ± 0.10	0.07	4	4
1580	01580	14.90	0.12	4.19 ± 0.06	0.11 ± 0.02	1.40 ± 0.00	1.03 ± 0.10	0.34	7	7
1580	01580	14.90	0.12	5.37 ± 0.04	0.07 ± 0.01	1.40 ± 0.00	1.61 ± 0.10	0.58	18	18
1620	01620	15.41	0.24	1.96 ± 0.06	0.32 ± 0.04	1.40 ± 0.00	1.78 ± 0.10	1.16	13	13
1685	01685	14.45	0.24	3.91 ± 0.08	0.19 ± 0.02	1.40 ± 0.00	1.68 ± 0.10	1.04	10	11
1980	01980	13.87	0.24	4.36 ± 0.10	0.26 ± 0.03	1.40 ± 0.00	1.83 ± 0.10	0.99	18	18
1980	01980	13.87	0.24	4.31 ± 0.18	0.27 ± 0.05	1.40 ± 0.00	1.94 ± 0.10	1.36	31	31
1980	01980	13.87	0.24	4.47 ± 0.14	0.25 ± 0.06	1.40 ± 0.00	1.97 ± 0.10	1.46	27	29
2062	02062	17.30	0.24	0.73 ± 0.03	0.39 ± 0.05	1.40 ± 0.00	1.46 ± 0.10	0.25	6	6
2063	02063	17.37	0.24	1.03 ± 0.03	0.19 ± 0.03	1.40 ± 0.00	0.93 ± 0.10	0.24	5	5
3691	03691	14.98	0.24	2.08 ± 0.09	0.42 ± 0.11	1.40 ± 0.00	1.19 ± 0.10	0.73	21	21
4055	04055	14.99	0.43	3.21 ± 0.16	0.17 ± 0.03	1.40 ± 0.00	1.70 ± 0.10	0.91	6	7
4183	04183	14.35	0.24	3.73 ± 0.15	0.23 ± 0.04	1.40 ± 0.00	1.21 ± 0.10	0.33	9	9
5646	05646	15.45	0.24	2.45 ± 0.06	0.19 ± 0.03	1.40 ± 0.00	1.32 ± 0.10	0.36	39	39
5646	05646	15.45	0.24	2.50 ± 0.05	0.19 ± 0.03	1.40 ± 0.00	1.28 ± 0.10	0.66	74	78
5646	05646	15.45	0.24	2.51 ± 0.05	0.18 ± 0.03	1.40 ± 0.00	1.41 ± 0.10	0.35	46	47
5731	05731	15.53	0.12	6.51 ± 3.14	0.03 ± 0.03	1.00 ± 0.51	1.60 ± 0.10	0.33	0	8
5828	05828	16.30	0.24	1.43 ± 0.06	0.26 ± 0.05	1.40 ± 0.00	1.29 ± 0.10	0.38	6	6
7335	07335	17.82	0.24	0.73 ± 0.02	0.25 ± 0.04	1.40 ± 0.00	1.52 ± 0.10	0.78	8	8
7350	07350	17.21	0.24	1.92 ± 0.03	0.06 ± 0.01	1.40 ± 0.00	1.06 ± 0.10	0.12	4	5
7889	07889	15.31	0.24	1.82 ± 0.08	0.40 ± 0.04	1.40 ± 0.00	1.27 ± 0.10	0.77	13	13
9202	09202	16.16	0.24	1.51 ± 0.05	0.27 ± 0.04	1.40 ± 0.00	1.29 ± 0.10	0.18	5	6
9400	09400	14.98	0.24	3.69 ± 0.05	0.13 ± 0.02	1.40 ± 0.00	2.13 ± 0.10	0.20	10	10
11066	11066	15.36	0.24	2.10 ± 0.09	0.29 ± 0.04	1.40 ± 0.00	1.83 ± 0.10	0.49	5	5
11405	11405	15.37	0.24	3.62 ± 0.05	0.10 ± 0.02	1.40 ± 0.00	2.67 ± 0.10	0.25	13	13
21088	21088	14.47	0.24	2.79 ± 0.10	0.37 ± 0.06	1.40 ± 0.00	1.63 ± 0.10	0.45	12	12
22099	22099	18.19	0.24	0.52 ± 0.11	0.35 ± 0.22	1.40 ± 0.40	1.60 ± 0.10	0.81	0	4
23606	23606	18.37	0.24	0.87 ± 0.01	0.11 ± 0.02	1.40 ± 0.00	2.46 ± 0.10	1.67	60	60
26817	26817	19.11	0.24	1.17 ± 0.53	0.03 ± 0.08	1.40 ± 0.52	1.60 ± 0.10	0.41	0	6
35107	35107	17.02	0.24	0.91 ± 0.03	0.33 ± 0.04	1.40 ± 0.00	1.41 ± 0.10	0.93	27	27
38086	38086	17.63	0.24	0.64 ± 0.19	0.39 ± 0.28	1.40 ± 0.50	1.60 ± 0.10	0.71	0	6
38091	38091	16.61	0.24	2.49 ± 0.03	0.06 ± 0.01	1.40 ± 0.00	2.30 ± 0.10	0.97	12	13

Table 4—Continued

Object	Packed	<i>H</i>	<i>G</i>	<i>d</i> (km)	<i>p_V</i>	η	<i>p_{IR}/p_V</i>	W2 amp.	<i>n_{W1}</i>	<i>n_{W2}</i>
52750	52750	16.74	0.24	0.96 ± 0.04	0.39 ± 0.06	1.40 ± 0.00	1.55 ± 0.10	0.73	22	24
52750	52750	16.74	0.24	0.93 ± 0.32	0.41 ± 0.25	1.40 ± 0.51	1.60 ± 0.10	0.19	0	5
53430	53430	16.85	0.24	1.34 ± 0.45	0.18 ± 0.17	1.40 ± 0.44	1.60 ± 0.10	0.78	0	10
68216	68216	16.66	0.24	0.99 ± 0.04	0.39 ± 0.06	1.40 ± 0.00	1.30 ± 0.10	0.38	8	8
68278	68278	18.50	0.12	1.46 ± 0.53	0.03 ± 0.03	1.40 ± 0.40	1.60 ± 0.10	0.52	0	23
85275	85275	16.45	0.24	2.50 ± 0.99	0.07 ± 0.06	1.40 ± 0.42	1.60 ± 0.10	0.53	0	14
85713	85713	16.01	0.24	3.03 ± 1.49	0.08 ± 0.12	1.40 ± 0.50	1.60 ± 0.10	0.37	0	6
85804	85804	15.47	0.24	2.27 ± 0.06	0.22 ± 0.04	1.40 ± 0.00	1.24 ± 0.10	0.17	11	11
85804	85804	15.47	0.24	2.19 ± 0.04	0.24 ± 0.02	1.40 ± 0.00	1.29 ± 0.10	0.21	13	14
85804	85804	15.47	0.24	2.84 ± 0.04	0.14 ± 0.02	1.40 ± 0.00	1.94 ± 0.10	0.58	21	22
85989	85989	17.03	0.24	1.60 ± 0.59	0.11 ± 0.17	1.40 ± 0.45	1.60 ± 0.10	0.39	0	4
86067	86067	16.52	0.24	1.50 ± 0.49	0.19 ± 0.14	1.40 ± 0.42	1.60 ± 0.10	0.54	0	11
86667	86667	17.59	0.24	0.74 ± 0.02	0.29 ± 0.05	1.40 ± 0.00	1.60 ± 0.10	0.76	4	4
86829	86829	16.11	0.24	1.81 ± 0.05	0.19 ± 0.03	1.40 ± 0.00	1.38 ± 0.10	0.13	6	6
88263	88263	15.73	0.24	5.10 ± 1.86	0.03 ± 0.04	1.40 ± 0.38	1.60 ± 0.10	0.93	0	18
88710	88710	18.14	0.34	0.75 ± 0.29	0.18 ± 0.14	1.40 ± 0.52	1.60 ± 0.10	0.99	0	71
90367	90367	18.11	0.24	2.06 ± 1.14	0.02 ± 0.07	1.40 ± 0.59	1.60 ± 0.10	0.48	0	13
90403	90403	17.78	0.24	0.57 ± 0.17	0.42 ± 0.24	1.40 ± 0.49	1.60 ± 0.10	0.49	0	5
90416	90416	18.58	0.24	0.98 ± 0.02	0.07 ± 0.01	1.40 ± 0.00	1.34 ± 0.10	0.07	5	5
100756	A0756	16.48	0.24	1.81 ± 0.04	0.14 ± 0.02	1.40 ± 0.00	1.80 ± 0.10	1.16	15	15
105140	A5140	15.81	0.24	1.97 ± 0.05	0.22 ± 0.04	1.40 ± 0.00	1.30 ± 0.10	0.58	8	9
108519	A8519	17.94	0.24	1.43 ± 0.54	0.06 ± 0.09	1.40 ± 0.46	1.60 ± 0.10	0.52	0	12
112985	B2985	15.66	0.24	3.65 ± 0.04	0.07 ± 0.01	1.40 ± 0.00	2.46 ± 0.10	0.12	11	11
112985	B2985	15.66	0.24	5.12 ± 0.03	0.04 ± 0.01	1.40 ± 0.00	2.80 ± 0.10	0.15	18	18
137084	D7084	16.52	0.24	1.23 ± 0.04	0.29 ± 0.04	1.40 ± 0.00	1.10 ± 0.10	0.48	4	4
137805	D7805	16.77	0.24	2.24 ± 0.03	0.07 ± 0.01	1.40 ± 0.00	1.40 ± 0.10	0.31	17	17
137925	D7925	16.25	0.24	1.36 ± 0.04	0.30 ± 0.05	1.40 ± 0.00	1.27 ± 0.10	0.29	4	5
140288	E0288	16.84	0.24	1.26 ± 0.03	0.20 ± 0.04	1.40 ± 0.00	1.03 ± 0.10	0.34	8	8
140288	E0288	16.84	0.24	1.21 ± 0.45	0.22 ± 0.23	1.40 ± 0.50	1.60 ± 0.10	0.74	0	5
141484	E1484	16.64	0.24	1.00 ± 0.04	0.39 ± 0.05	1.40 ± 0.00	1.44 ± 0.10	0.26	8	9
141484	E1484	16.64	0.24	1.02 ± 0.03	0.37 ± 0.04	1.40 ± 0.00	1.59 ± 0.10	0.39	16	16
142040	E2040	16.31	0.24	1.26 ± 0.04	0.34 ± 0.04	1.40 ± 0.00	1.71 ± 0.10	0.36	43	44

Table 4—Continued

Object	Packed	<i>H</i>	<i>G</i>	<i>d</i> (km)	<i>p_V</i>	η	<i>p_{IR}/p_V</i>	W2 amp.	<i>n_{W1}</i>	<i>n_{W2}</i>
152679	F2679	16.43	0.12	4.18 ± 0.01	0.03 ± 0.00	1.40 ± 0.00	7.21 ± 0.10	1.22	29	29
152978	F2978	19.73	0.24	0.32 ± 0.07	0.23 ± 0.13	1.40 ± 0.32	1.60 ± 0.10	0.74	0	8
152978	F2978	19.73	0.24	0.37 ± 0.14	0.17 ± 0.14	1.40 ± 0.47	1.60 ± 0.10	0.57	0	5
153195	F3195	17.94	0.24	1.32 ± 0.55	0.07 ± 0.07	1.40 ± 0.47	1.60 ± 0.10	0.77	0	14
153195	F3195	17.94	0.24	1.60 ± 0.59	0.05 ± 0.04	1.40 ± 0.39	1.60 ± 0.10	0.45	0	7
154807	F4807	18.72	0.24	0.47 ± 0.01	0.26 ± 0.03	1.40 ± 0.00	1.69 ± 0.10	0.92	14	15
155110	F5110	17.66	0.24	0.68 ± 0.03	0.33 ± 0.04	1.40 ± 0.00	1.87 ± 0.10	0.34	6	6
155110	F5110	17.66	0.24	0.75 ± 0.32	0.27 ± 0.23	1.40 ± 0.54	1.60 ± 0.10	0.37	0	5
159459	F9459	15.98	0.24	1.83 ± 0.09	0.21 ± 0.03	1.40 ± 0.00	1.11 ± 0.10	0.38	5	6
159504	F9504	16.99	0.05	2.31 ± 0.02	0.05 ± 0.01	1.40 ± 0.00	1.73 ± 0.10	0.24	9	9
159686	F9686	16.65	0.24	1.80 ± 0.03	0.12 ± 0.02	1.40 ± 0.00	3.56 ± 0.10	0.28	8	9
159929	F9929	17.75	0.24	2.62 ± 1.20	0.02 ± 0.08	1.40 ± 0.45	1.60 ± 0.10	0.34	0	8
161989	G1989	17.43	0.24	0.64 ± 0.02	0.46 ± 0.09	1.40 ± 0.00	1.81 ± 0.10	1.16	64	69
162080	G2080	19.89	0.24	0.68 ± 0.32	0.04 ± 0.05	1.40 ± 0.55	1.60 ± 0.10	0.94	0	20
162463	G2463	17.99	0.24	0.93 ± 0.35	0.13 ± 0.21	1.40 ± 0.49	1.60 ± 0.10	0.85	0	21
162463	G2463	17.99	0.24	0.98 ± 0.35	0.12 ± 0.14	1.40 ± 0.43	1.60 ± 0.10	0.40	0	6
162567	G2567	20.18	0.24	0.29 ± 0.12	0.18 ± 0.16	1.40 ± 0.56	1.60 ± 0.10	0.19	0	5
163760	G3760	16.53	0.24	2.35 ± 0.77	0.08 ± 0.08	1.40 ± 0.39	1.60 ± 0.10	0.40	0	9
163899	G3899	17.36	0.24	0.80 ± 0.02	0.31 ± 0.04	1.40 ± 0.00	1.35 ± 0.10	1.97	24	24
164206	G4206	17.86	0.24	1.13 ± 0.55	0.10 ± 0.09	1.40 ± 0.55	1.60 ± 0.10	0.94	0	8
172034	H2034	17.67	0.24	0.66 ± 0.17	0.34 ± 0.25	1.40 ± 0.44	1.60 ± 0.10	1.17	0	24
173689	H3689	18.28	0.24	0.73 ± 0.29	0.16 ± 0.19	1.40 ± 0.55	1.60 ± 0.10	0.17	0	5
190161	J0161	16.67	0.24	3.05 ± 0.02	0.04 ± 0.01	1.40 ± 0.00	1.79 ± 0.10	0.36	28	30
200754	K0754	18.67	0.24	0.56 ± 0.21	0.19 ± 0.15	1.40 ± 0.52	1.60 ± 0.10	0.29	0	5
206378	K6378	18.68	0.06	0.37 ± 0.02	0.44 ± 0.19	1.40 ± 0.00	1.85 ± 0.10	0.75	20	20
212359	L2359	16.98	0.24	1.25 ± 0.40	0.18 ± 0.18	1.40 ± 0.42	1.60 ± 0.10	0.33	0	9
237805	N7805	17.63	0.24	0.69 ± 0.26	0.33 ± 0.22	1.40 ± 0.57	1.60 ± 0.10	1.47	0	45
241662	O1662	17.64	0.24	0.91 ± 0.02	0.19 ± 0.03	1.40 ± 0.00	1.56 ± 0.10	0.38	10	10
241662	O1662	17.64	0.24	0.81 ± 0.26	0.24 ± 0.22	1.40 ± 0.47	1.60 ± 0.10	0.44	0	8
248590	O8590	16.82	0.24	3.35 ± 1.04	0.03 ± 0.03	0.80 ± 0.40	1.50 ± 0.10	0.27	0	13
256412	P6412	17.17	0.24	2.90 ± 0.02	0.03 ± 0.01	1.00 ± 0.20	4.06 ± 0.10	0.57	15	15
275611	R5611	18.24	0.24	1.48 ± 0.01	0.04 ± 0.01	1.40 ± 0.00	2.67 ± 0.10	0.70	24	25

Table 4—Continued

Object	Packed	<i>H</i>	<i>G</i>	<i>d</i> (km)	<i>p_V</i>	η	<i>p_{IR}/p_V</i>	W2 amp.	<i>n_{W1}</i>	<i>n_{W2}</i>
276049	R6049	16.50	0.12	2.24 ± 0.02	0.09 ± 0.02	1.00 ± 0.20	0.23 ± 0.10	0.24	11	11
276049	R6049	16.50	0.12	4.71 ± 2.84	0.02 ± 0.04	1.00 ± 0.60	1.60 ± 0.10	0.37	0	12
276786	R6786	18.11	0.24	1.72 ± 0.68	0.03 ± 0.07	1.40 ± 0.45	1.60 ± 0.10	0.85	0	12
285331	S5331	18.47	0.24	0.66 ± 0.01	0.17 ± 0.02	1.40 ± 0.00	2.04 ± 0.10	0.32	6	6
285331	S5331	18.47	0.24	0.65 ± 0.01	0.17 ± 0.02	1.40 ± 0.00	1.96 ± 0.10	0.65	10	10
294739	T4739	17.39	0.24	0.74 ± 0.21	0.36 ± 0.19	1.40 ± 0.46	1.60 ± 0.10	0.35	0	7
297274	T7274	16.90	0.24	1.21 ± 0.03	0.21 ± 0.03	1.40 ± 0.00	1.01 ± 0.10	0.64	5	5
303450	U3450	20.86	0.24	0.18 ± 0.06	0.24 ± 0.12	1.40 ± 0.43	1.60 ± 0.10	0.62	0	7
307493	U7493	18.95	0.24	1.43 ± 0.09	0.02 ± 0.00	1.22 ± 0.06	1.60 ± 0.10	0.34	10	10
311554	V1554	18.80	0.24	0.38 ± 0.02	0.36 ± 0.05	1.40 ± 0.00	2.07 ± 0.10	0.72	7	8
326388	W6388	18.26	0.24	1.15 ± 0.01	0.07 ± 0.01	1.40 ± 0.00	0.70 ± 0.10	0.39	11	12
337248	X7248	20.00	0.15	0.85 ± 0.06	0.02 ± 0.01	1.40 ± 0.09	4.79 ± 0.10	1.01	6	6
337248	X7248	20.00	0.15	0.61 ± 0.26	0.05 ± 0.06	1.40 ± 0.49	1.60 ± 0.10	0.34	0	7
345646	Y5646	19.90	0.15	0.41 ± 0.01	0.12 ± 0.02	1.40 ± 0.00	8.52 ± 0.10	0.42	6	7
355770	Z5770	18.40	0.15	1.20 ± 0.49	0.05 ± 0.08	1.40 ± 0.48	1.60 ± 0.10	1.68	0	57
363027	a3027	19.50	0.15	0.58 ± 0.27	0.08 ± 0.11	1.40 ± 0.54	1.60 ± 0.10	0.30	0	4
363027	a3027	19.50	0.15	0.69 ± 0.25	0.06 ± 0.07	1.40 ± 0.46	1.60 ± 0.10	0.19	0	6
363505	a3505	18.10	0.15	1.88 ± 0.01	0.03 ± 0.00	1.40 ± 0.00	2.63 ± 0.10	0.70	26	28
373135	b3135	19.50	0.15	1.05 ± 0.36	0.03 ± 0.01	1.40 ± 0.38	1.60 ± 0.10	0.88	0	4
381906	c1906	17.90	0.15	0.52 ± 0.10	0.45 ± 0.27	1.40 ± 0.39	1.60 ± 0.10	0.43	0	5
385186	c5186	17.70	0.15	0.81 ± 0.02	0.22 ± 0.03	1.40 ± 0.00	2.04 ± 0.10	0.57	9	9
385186	c5186	17.70	0.15	0.97 ± 0.29	0.16 ± 0.15	1.40 ± 0.41	1.60 ± 0.10	0.43	0	20
401857	e1857	16.10	0.15	4.28 ± 0.04	0.03 ± 0.01	1.40 ± 0.00	2.28 ± 0.10	0.43	6	6
401857	e1857	16.10	0.15	3.90 ± 1.87	0.04 ± 0.07	1.40 ± 0.47	1.60 ± 0.10	0.78	0	11
401925	e1925	18.40	0.15	0.48 ± 0.10	0.34 ± 0.19	1.40 ± 0.37	1.60 ± 0.10	0.43	0	5
413123	f3123	19.00	0.15	1.22 ± 0.50	0.03 ± 0.05	1.40 ± 0.45	1.60 ± 0.10	0.89	0	29
413123	f3123	19.00	0.15	1.26 ± 0.52	0.03 ± 0.08	1.40 ± 0.46	1.60 ± 0.10	0.44	0	12
413192	f3192	16.80	0.15	2.78 ± 0.02	0.04 ± 0.01	1.40 ± 0.00	1.31 ± 0.10	0.33	23	25
413192	f3192	16.80	0.15	2.16 ± 0.02	0.07 ± 0.01	1.40 ± 0.00	1.49 ± 0.10	0.84	114	118
414287	f4287	17.70	0.15	1.97 ± 0.74	0.04 ± 0.04	1.40 ± 0.41	1.60 ± 0.10	0.57	0	9
414772	f4772	19.00	0.15	1.00 ± 0.68	0.04 ± 0.06	1.00 ± 0.73	1.60 ± 0.10	0.95	0	5
415711	f5711	19.00	0.15	0.35 ± 0.10	0.37 ± 0.26	1.40 ± 0.46	1.60 ± 0.10	0.66	0	9

Table 4—Continued

Object	Packed	<i>H</i>	<i>G</i>	<i>d</i> (km)	<i>p_V</i>	η	<i>p_{IR}/p_V</i>	W2 amp.	<i>n_{W1}</i>	<i>n_{W2}</i>
415986	f5986	18.10	0.15	1.07 ± 0.54	0.09 ± 0.11	1.40 ± 0.57	1.60 ± 0.10	0.50	0	10
415986	f5986	18.10	0.15	1.08 ± 0.29	0.09 ± 0.08	1.40 ± 0.33	1.60 ± 0.10	0.87	0	27
416071	f6071	17.90	0.15	0.80 ± 0.01	0.19 ± 0.03	1.40 ± 0.00	2.24 ± 0.10	0.33	8	8
417264	f7264	17.20	0.15	1.93 ± 0.02	0.06 ± 0.01	1.40 ± 0.00	2.16 ± 0.10	0.68	15	15
417264	f7264	17.20	0.15	1.93 ± 0.01	0.06 ± 0.01	1.40 ± 0.00	2.59 ± 0.10	0.88	27	27
417264	f7264	17.20	0.15	2.72 ± 1.26	0.03 ± 0.04	1.40 ± 0.43	1.60 ± 0.10	0.84	0	11
418797	f8797	19.50	0.15	0.79 ± 0.23	0.05 ± 0.06	1.40 ± 0.36	1.60 ± 0.10	0.39	0	7
422699	g2699	18.30	0.15	0.62 ± 0.24	0.22 ± 0.18	1.40 ± 0.52	1.60 ± 0.10	0.97	0	11
424089	g4089	17.70	0.15	2.31 ± 0.72	0.03 ± 0.03	1.40 ± 0.32	1.60 ± 0.10	0.49	0	11
424392	g4392	21.90	0.15	0.24 ± 0.10	0.05 ± 0.06	1.40 ± 0.49	1.60 ± 0.10	0.46	0	9
428223	g8223	16.10	0.15	2.53 ± 0.82	0.10 ± 0.13	1.40 ± 0.37	1.60 ± 0.10	0.67	0	10
429746	g9746	17.30	0.15	1.27 ± 0.50	0.13 ± 0.10	1.40 ± 0.42	1.60 ± 0.10	0.55	0	8
431107	h1107	17.70	0.15	1.27 ± 0.44	0.09 ± 0.15	1.40 ± 0.43	1.60 ± 0.10	0.66	0	8
433953	h3953	20.90	0.15	0.26 ± 0.09	0.11 ± 0.13	1.40 ± 0.44	1.60 ± 0.10	0.80	0	7
433992	h3992	18.00	0.15	0.88 ± 0.02	0.14 ± 0.02	1.40 ± 0.00	2.52 ± 0.10	0.38	5	5
434096	h4096	18.00	0.15	0.53 ± 0.02	0.43 ± 0.08	1.40 ± 0.00	2.32 ± 0.10	0.82	4	6
434633	h4633	20.90	0.15	0.31 ± 0.12	0.08 ± 0.09	1.40 ± 0.45	1.60 ± 0.10	0.31	0	6
434633	h4633	20.90	0.15	0.44 ± 0.14	0.04 ± 0.02	1.40 ± 0.37	1.60 ± 0.10	0.37	0	13
436671	h6671	18.00	0.15	2.16 ± 0.02	0.02 ± 0.01	1.40 ± 0.00	4.24 ± 0.10	0.44	7	7
437879	h7879	17.70	0.15	2.24 ± 0.95	0.03 ± 0.06	1.40 ± 0.45	1.60 ± 0.10	0.87	0	13
437994	h7994	17.30	0.15	0.80 ± 0.21	0.33 ± 0.16	1.40 ± 0.38	1.60 ± 0.10	0.87	0	11
438990	h8990	18.30	0.15	0.82 ± 0.37	0.13 ± 0.16	1.40 ± 0.53	1.60 ± 0.10	0.48	0	5
439889	h9889	20.10	0.15	0.59 ± 0.18	0.05 ± 0.04	1.40 ± 0.38	1.60 ± 0.10	0.31	0	4
442605	i2605	19.10	0.15	0.44 ± 0.11	0.21 ± 0.17	1.40 ± 0.37	1.60 ± 0.10	0.50	0	5
442742	i2742	17.60	0.15	2.00 ± 0.01	0.04 ± 0.01	1.40 ± 0.00	2.83 ± 0.10	0.92	71	78
443806	i3806	22.00	0.15	0.29 ± 0.12	0.03 ± 0.04	1.40 ± 0.52	1.60 ± 0.10	0.24	0	12
443880	i3880	19.40	0.15	0.25 ± 0.04	0.50 ± 0.17	1.80 ± 0.55	1.60 ± 0.10	0.65	0	6
443923	i3923	17.40	0.15	2.15 ± 1.01	0.04 ± 0.07	1.00 ± 0.58	1.60 ± 0.10	0.52	0	11
445025	i5025	17.50	0.15	2.10 ± 0.02	0.04 ± 0.01	1.40 ± 0.00	0.70 ± 0.10	0.09	5	5
445305	i5305	19.90	0.15	0.80 ± 0.31	0.03 ± 0.05	1.40 ± 0.45	1.60 ± 0.10	0.20	0	4
450159	j0159	18.90	0.15	0.73 ± 0.23	0.09 ± 0.10	1.40 ± 0.40	1.60 ± 0.10	0.62	0	5
453687	j3687	19.30	0.15	1.06 ± 0.48	0.03 ± 0.03	1.40 ± 0.47	1.60 ± 0.10	0.25	0	13

Table 4—Continued

Object	Packed	<i>H</i>	<i>G</i>	<i>d</i> (km)	<i>p_V</i>	η	<i>p_{IR}/p_V</i>	W2 amp.	<i>n_{W1}</i>	<i>n_{W2}</i>
453707	j3707	18.60	0.15	0.50 ± 0.14	0.26 ± 0.12	1.40 ± 0.39	1.60 ± 0.10	0.40	0	4
454078	j4078	17.50	0.15	2.96 ± 1.20	0.02 ± 0.04	1.40 ± 0.44	1.60 ± 0.10	0.23	0	15
454100	j4100	20.10	0.15	0.55 ± 0.01	0.05 ± 0.01	1.40 ± 0.00	1.70 ± 0.10	0.26	6	6
2002 GP186	K02GI6P	20.30	0.15	0.17 ± 0.05	0.44 ± 0.27	1.40 ± 0.48	1.60 ± 0.10	0.29	0	5
2003 KZ18	K03K18Z	21.20	0.15	0.47 ± 0.19	0.03 ± 0.04	1.40 ± 0.48	1.60 ± 0.10	0.69	0	6
2003 MT9	K03M09T	18.60	0.15	0.68 ± 0.22	0.14 ± 0.17	1.40 ± 0.46	1.60 ± 0.10	0.30	0	4
2006 KL89	K06K89L	18.60	0.15	0.96 ± 0.38	0.07 ± 0.03	1.40 ± 0.41	1.60 ± 0.10	0.68	0	23
2006 KL89	K06K89L	18.60	0.15	1.07 ± 0.52	0.06 ± 0.10	1.40 ± 0.53	1.60 ± 0.10	0.65	0	15
2006 OF5	K06O05F	19.30	0.15	0.95 ± 0.55	0.04 ± 0.03	1.00 ± 0.64	1.60 ± 0.10	0.63	0	46
2006 OF5	K06O05F	19.30	0.15	0.93 ± 0.32	0.04 ± 0.03	1.00 ± 0.49	1.60 ± 0.10	0.43	0	47
2006 UR217	K06UL7R	19.80	0.15	0.89 ± 0.07	0.03 ± 0.01	1.40 ± 0.11	6.16 ± 0.10	0.26	8	9
2006 UR217	K06UL7R	19.80	0.15	0.95 ± 0.40	0.02 ± 0.05	1.40 ± 0.47	1.60 ± 0.10	0.44	0	6
2007 WE55	K07W55E	20.20	0.15	0.69 ± 0.18	0.03 ± 0.05	1.40 ± 0.33	1.60 ± 0.10	0.78	0	13
2010 CO1	K10C01O	21.80	0.15	0.29 ± 0.15	0.04 ± 0.06	1.00 ± 0.67	1.60 ± 0.10	0.43	0	13
2010 LF86	K10L86F	17.20	0.15	2.56 ± 1.22	0.04 ± 0.05	1.40 ± 0.50	1.60 ± 0.10	0.49	0	5
2010 UB8	K10U08B	19.60	0.15	0.92 ± 0.08	0.03 ± 0.01	1.16 ± 0.09	1.60 ± 0.10	0.16	7	7
2010 UB8	K10U08B	19.60	0.15	0.88 ± 0.42	0.03 ± 0.05	1.00 ± 0.61	1.60 ± 0.10	0.37	0	15
2010 YD3	K10Y03D	20.00	0.15	0.76 ± 0.35	0.03 ± 0.04	1.40 ± 0.52	1.60 ± 0.10	0.54	0	12
2011 AM24	K11A24M	20.50	0.15	0.50 ± 0.01	0.04 ± 0.01	1.40 ± 0.01	0.47 ± 0.10	0.49	8	8
2011 AM24	K11A24M	20.50	0.15	0.51 ± 0.01	0.04 ± 0.01	1.40 ± 0.01	0.94 ± 0.10	0.47	14	15
2011 HJ61	K11H61J	19.30	0.15	1.28 ± 0.57	0.02 ± 0.04	1.40 ± 0.47	1.60 ± 0.10	0.97	0	13
2011 JU2	K11J02U	18.40	0.15	1.49 ± 0.56	0.03 ± 0.06	1.40 ± 0.42	1.60 ± 0.10	0.77	0	4
2011 OL5	K11O05L	20.20	0.15	0.28 ± 0.08	0.19 ± 0.16	1.40 ± 0.42	1.60 ± 0.10	1.05	0	36
2011 OL5	K11O05L	20.20	0.15	0.28 ± 0.11	0.19 ± 0.16	1.40 ± 0.51	1.60 ± 0.10	0.60	0	13
2011 VQ5	K11V05Q	20.10	0.15	0.56 ± 0.23	0.05 ± 0.08	1.40 ± 0.50	1.60 ± 0.10	0.85	0	18
2011 YB40	K11Y40B	19.10	0.15	0.42 ± 0.12	0.22 ± 0.17	1.40 ± 0.42	1.60 ± 0.10	0.38	0	5
2012 OD1	K12O01D	18.60	0.15	0.35 ± 0.09	0.54 ± 0.26	1.40 ± 0.44	1.60 ± 0.10	0.36	0	5
2014 JY24	K14J24Y	18.30	0.15	1.92 ± 1.01	0.02 ± 0.05	1.40 ± 0.55	1.60 ± 0.10	0.37	0	15
2014 QK434	K14Qh4K	19.10	0.15	0.30 ± 0.01	0.46 ± 0.05	1.40 ± 0.00	0.83 ± 0.10	0.41	5	5
2014 TA36	K14T36A	20.70	0.15	0.55 ± 0.23	0.03 ± 0.03	1.40 ± 0.49	1.60 ± 0.10	0.69	0	11
2014 US	K14U00S	19.10	0.15	0.47 ± 0.15	0.19 ± 0.26	1.40 ± 0.46	1.60 ± 0.10	0.30	0	16
2014 US	K14U00S	19.10	0.15	0.56 ± 0.19	0.13 ± 0.08	1.40 ± 0.42	1.60 ± 0.10	0.38	0	14

Table 4—Continued

Object	Packed	<i>H</i>	<i>G</i>	<i>d</i> (km)	<i>p_V</i>	η	<i>p_{IR}</i> / <i>p_V</i>	W2 amp.	<i>n_{W1}</i>	<i>n_{W2}</i>
2014 UV33	K14U33V	17.90	0.15	0.82 ± 0.02	0.18 ± 0.03	1.40 ± 0.00	3.29 ± 0.10	1.58	20	24
2014 UF206	K14UK6F	18.80	0.15	1.52 ± 0.68	0.02 ± 0.02	1.00 ± 0.53	1.60 ± 0.10	0.68	0	46
2014 UF206	K14UK6F	18.80	0.15	1.29 ± 0.06	0.03 ± 0.01	1.12 ± 0.05	1.60 ± 0.10	0.16	23	23
2014 WF365	K14Wa5F	17.20	0.15	2.18 ± 0.02	0.05 ± 0.01	1.40 ± 0.00	1.39 ± 0.10	0.20	7	7
2014 XR6	K14X06R	18.30	0.15	0.86 ± 0.29	0.11 ± 0.17	1.40 ± 0.45	1.60 ± 0.10	0.56	0	10
2014 XX31	K14X31X	17.50	0.15	1.49 ± 0.53	0.08 ± 0.06	1.40 ± 0.39	1.60 ± 0.10	0.67	0	6
2014 YJ14	K14Y14J	18.30	0.15	1.91 ± 0.12	0.02 ± 0.01	1.12 ± 0.06	1.60 ± 0.10	0.12	7	7
2014 YS14	K14Y14S	21.10	0.15	0.30 ± 0.12	0.07 ± 0.09	1.40 ± 0.51	1.60 ± 0.10	0.57	0	5
2014 YT14	K14Y14T	18.90	0.15	1.16 ± 0.47	0.04 ± 0.02	1.00 ± 0.52	1.60 ± 0.10	0.95	0	18
2014 YS34	K14Y34S	20.80	0.15	0.13 ± 0.03	0.50 ± 0.23	1.40 ± 0.41	1.60 ± 0.10	0.46	0	5
2014 YB35	K14Y35B	19.00	0.15	0.28 ± 0.01	0.57 ± 0.07	1.40 ± 0.00	1.31 ± 0.10	0.52	6	6
2014 YR43	K14Y43R	19.50	0.15	0.37 ± 0.13	0.20 ± 0.13	1.40 ± 0.47	1.60 ± 0.10	0.36	0	9
2015 AC17	K15A17C	19.90	0.15	0.67 ± 0.28	0.04 ± 0.04	1.00 ± 0.57	1.60 ± 0.10	0.67	0	34
2015 AY245	K15AO5Y	21.20	0.15	0.37 ± 0.03	0.04 ± 0.02	1.40 ± 0.12	8.64 ± 0.10	0.43	13	13
2015 AY245	K15AO5Y	21.20	0.15	0.39 ± 0.18	0.04 ± 0.09	1.40 ± 0.59	1.60 ± 0.10	2.84	0	60
2015 AK280	K15AS0K	21.80	0.15	0.36 ± 0.12	0.03 ± 0.04	1.40 ± 0.41	1.60 ± 0.10	0.36	0	4
2015 BY516	K15Bp6Y	22.30	0.15	0.24 ± 0.12	0.04 ± 0.03	1.00 ± 0.64	1.60 ± 0.10	0.55	0	8
2015 CV13	K15C13V	20.30	0.15	0.44 ± 0.13	0.07 ± 0.04	1.40 ± 0.35	1.60 ± 0.10	0.69	0	8
2015 DE176	K15DH6E	19.70	0.15	0.68 ± 0.04	0.05 ± 0.01	1.40 ± 0.07	0.21 ± 0.10	0.19	9	9
2015 DE176	K15DH6E	19.70	0.15	0.57 ± 0.29	0.07 ± 0.11	1.40 ± 0.59	1.60 ± 0.10	0.25	0	4
2015 DX198	K15DJ8X	22.00	0.15	0.35 ± 0.10	0.02 ± 0.02	1.40 ± 0.38	1.60 ± 0.10	1.31	0	9
2015 EZ	K15E00Z	20.30	0.15	0.19 ± 0.05	0.36 ± 0.19	1.40 ± 0.39	1.60 ± 0.10	0.62	0	10
2015 FZ35	K15F35Z	19.40	0.15	0.64 ± 0.21	0.08 ± 0.11	1.40 ± 0.41	1.60 ± 0.10	0.57	0	5
2015 FY117	K15FB7Y	21.30	0.15	0.38 ± 0.17	0.04 ± 0.04	1.00 ± 0.60	1.60 ± 0.10	0.62	0	43
2015 FH120	K15FC0H	18.70	0.15	0.75 ± 0.26	0.11 ± 0.11	1.40 ± 0.46	1.60 ± 0.10	0.25	0	11
2015 FU332	K15FX2U	17.20	0.15	0.94 ± 0.36	0.26 ± 0.27	1.40 ± 0.53	1.60 ± 0.10	0.47	0	9
2015 FD341	K15FY1D	17.70	0.15	1.25 ± 0.48	0.09 ± 0.08	1.40 ± 0.43	1.60 ± 0.10	0.77	0	4
2015 FT344	K15FY4T	19.90	0.15	0.75 ± 0.24	0.03 ± 0.03	1.40 ± 0.39	1.60 ± 0.10	0.60	0	4
2015 FT344	K15FY4T	19.90	0.15	0.76 ± 0.21	0.03 ± 0.04	1.40 ± 0.34	1.60 ± 0.10	0.46	0	7
2015 GY	K15G00Y	21.70	0.15	0.14 ± 0.05	0.18 ± 0.19	1.40 ± 0.50	1.60 ± 0.10	0.24	0	4
2015 GK50	K15G50K	20.60	0.15	0.61 ± 0.30	0.03 ± 0.03	1.00 ± 0.62	1.60 ± 0.10	0.48	0	9
2015 GK50	K15G50K	20.60	0.15	0.46 ± 0.03	0.05 ± 0.01	0.99 ± 0.06	1.60 ± 0.10	0.27	16	16

Table 4—Continued

Object	Packed	<i>H</i>	<i>G</i>	<i>d</i> (km)	<i>p_V</i>	η	<i>p_{IR}/p_V</i>	W2 amp.	<i>n_{W1}</i>	<i>n_{W2}</i>
2015 GN50	K15G50N	20.20	0.15	0.29 ± 0.11	0.18 ± 0.12	1.40 ± 0.46	1.60 ± 0.10	0.36	0	5
2015 HF11	K15H11F	19.40	0.15	1.11 ± 0.44	0.02 ± 0.01	1.40 ± 0.42	1.60 ± 0.10	0.82	0	10
2015 JF11	K15J11F	21.20	0.15	0.17 ± 0.05	0.20 ± 0.11	1.40 ± 0.40	1.60 ± 0.10	0.34	0	6
2015 KH157	K15KF7H	20.00	0.15	0.58 ± 0.23	0.05 ± 0.11	1.40 ± 0.49	1.60 ± 0.10	0.22	0	9
2015 KL157	K15KF7L	19.10	0.15	1.45 ± 0.31	0.02 ± 0.01	1.00 ± 0.38	1.50 ± 0.10	0.76	0	48
2015 KL157	K15KF7L	19.10	0.15	0.36 ± 0.01	0.30 ± 0.05	0.40 ± 0.00	1.50 ± 0.10	1.05	9	12
2015 LK24	K15L24K	21.60	0.15	0.31 ± 0.11	0.04 ± 0.07	1.40 ± 0.44	1.60 ± 0.10	0.39	0	8
2015 MQ130	K15MD0Q	20.90	0.15	0.36 ± 0.07	0.06 ± 0.03	0.54 ± 0.10	1.60 ± 0.10	0.36	5	7
2015 MQ130	K15MD0Q	20.90	0.15	0.55 ± 0.26	0.03 ± 0.03	1.00 ± 0.61	1.60 ± 0.10	0.83	0	4
2015 NA14	K15N14A	22.00	0.15	0.09 ± 0.02	0.34 ± 0.18	1.40 ± 0.32	1.60 ± 0.10	0.45	0	5
2015 OA22	K15O22A	20.00	0.15	0.79 ± 0.34	0.03 ± 0.03	1.00 ± 0.56	1.60 ± 0.10	0.11	0	4
2015 OS35	K15O35S	19.10	0.15	1.26 ± 0.01	0.03 ± 0.00	1.40 ± 0.00	5.95 ± 0.10	0.17	20	22
2015 OS35	K15O35S	19.10	0.15	1.42 ± 0.01	0.02 ± 0.00	1.40 ± 0.00	6.34 ± 0.10	0.15	10	10
2015 PD	K15P00D	19.30	0.15	0.62 ± 0.22	0.09 ± 0.10	1.40 ± 0.44	1.60 ± 0.10	0.57	0	8
2015 PM57	K15P57M	18.60	0.15	0.59 ± 0.21	0.19 ± 0.22	1.40 ± 0.49	1.60 ± 0.10	0.22	0	7
2015 QM3	K15Q03M	20.30	0.15	0.27 ± 0.05	0.19 ± 0.15	1.40 ± 0.27	1.60 ± 0.10	0.61	0	9
2015 RS83	K15R83S	19.40	0.15	0.47 ± 0.13	0.14 ± 0.13	1.40 ± 0.37	1.60 ± 0.10	0.52	0	5
2015 RR150	K15RF0R	19.70	0.15	0.34 ± 0.12	0.20 ± 0.19	1.40 ± 0.46	1.60 ± 0.10	0.60	0	13
2015 SF20	K15S20F	19.70	0.15	0.40 ± 0.16	0.15 ± 0.14	1.40 ± 0.53	1.60 ± 0.10	0.52	0	8
2015 SS20	K15S20S	22.40	0.15	0.26 ± 0.10	0.03 ± 0.03	1.40 ± 0.46	1.60 ± 0.10	0.44	0	7
2015 TK237	K15TN7K	22.60	0.15	0.23 ± 0.07	0.03 ± 0.04	1.40 ± 0.40	1.60 ± 0.10	0.53	0	7
2015 TW346	K15TY6W	18.60	0.15	1.26 ± 0.46	0.04 ± 0.04	1.40 ± 0.41	1.60 ± 0.10	0.44	0	15
2015 UK52	K15U52K	20.10	0.15	0.21 ± 0.06	0.35 ± 0.22	1.40 ± 0.45	1.60 ± 0.10	0.34	0	5
2015 VZ145	K15VE5Z	23.70	0.15	0.16 ± 0.06	0.02 ± 0.05	1.40 ± 0.52	1.60 ± 0.10	1.36	0	5
2015 WM16	K15W16M	21.80	0.15	0.39 ± 0.06	0.02 ± 0.01	1.10 ± 0.16	1.60 ± 0.10	0.17	8	8
2015 XB130	K15XD0B	21.80	0.15	0.33 ± 0.13	0.03 ± 0.04	1.40 ± 0.48	1.60 ± 0.10	0.58	0	9
2015 XY378	K15Xb8Y	19.60	0.15	0.31 ± 0.11	0.26 ± 0.23	1.40 ± 0.46	1.60 ± 0.10	0.32	0	5

Table 5. Measured diameters (d) and albedos (p_V) of non-NEA asteroids observed during Year 2 of the NEOWISE Reactivation mission. Asteroids may be identified by numbers, provisional designations, or via the MPC packed format. Beaming η , H , G , the amplitude of the $4.6 \mu\text{m}$ light curve (W2 amp., in mag), and the numbers of observations used in the $3.4 \mu\text{m}$ (n_{W1}) and $4.6 \mu\text{m}$ (n_{W2}) wavelengths are also reported. Only the first 10 lines are shown; the remainder are available in electronic format through the journal website.

Object	Packed	H	G	d (km)	p_V	η	p_{IR}/p_V	W2 amp.	n_{W1}	n_{W2}
10	00010	5.46	0.12	450.53 ± 200.23	0.05 ± 0.05	0.95 ± 0.23	1.50 ± 0.10	0.05	4	4
13	00013	6.77	0.12	207.98 ± 46.68	0.08 ± 0.04	1.00 ± 0.35	1.00 ± 0.60	0.16	5	5
13	00013	6.77	0.12	192.79 ± 53.36	0.09 ± 0.06	1.00 ± 0.39	1.00 ± 0.60	0.32	9	9
19	00019	7.20	0.12	176.97 ± 56.71	0.06 ± 0.07	0.95 ± 0.21	1.50 ± 0.10	0.25	10	10
19	00019	7.20	0.12	182.71 ± 40.61	0.06 ± 0.03	0.95 ± 0.14	1.50 ± 0.10	0.32	8	8
21	00021	7.45	0.24	102.07 ± 24.56	0.18 ± 0.08	1.00 ± 0.39	1.00 ± 0.60	0.50	11	11
21	00021	7.45	0.24	99.71 ± 22.62	0.18 ± 0.05	1.00 ± 0.38	1.00 ± 0.60	0.35	12	13
23	00023	7.09	0.24	93.99 ± 20.14	0.29 ± 0.14	0.95 ± 0.20	1.50 ± 0.10	0.23	9	9
30	00030	7.67	0.24	105.70 ± 23.25	0.19 ± 0.11	0.95 ± 0.19	1.50 ± 0.10	0.23	6	7
33	00033	8.60	0.24	54.39 ± 11.84	0.23 ± 0.13	0.95 ± 0.19	1.50 ± 0.10	0.36	7	7

Table 6. Measured diameters and albedos for objects observed during the Year 2 Reactivation mission that may be accessible by spacecraft, following the NHATS criteria. Also listed is the minimum mission round trip time in days for each object from Barbee et al. (2013).

Number	Designation	D (km)	p_V	Minimum round trip (days)
(35107)	1991 VH	0.91 ± 0.03	0.33 ± 0.04	354
(163899)	2003 SD220	0.80 ± 0.02	0.31 ± 0.04	122
(363505)	2003 UC20	1.88 ± 0.01	0.03 ± 0.00	290
(424392)	2007 YJ	0.24 ± 0.10	0.05 ± 0.06	98
	2011 AM24	0.50 ± 0.01	0.04 ± 0.01	130
	2015 GY	0.14 ± 0.05	0.18 ± 0.19	346
	2015 NA14	0.09 ± 0.02	0.34 ± 0.18	170